Generation of Synthetic Image Datasets for Time-Lapse Fluorescence Microscopy

David Svoboda and Vladimír Ulman

Centre for Biomedical Image Analysis, Masaryk University,
Brno, 60200, Czech Republic
{svoboda,ulman}@fi.muni.cz
http://cbia.fi.muni.cz

Abstract. In the field of biomedical image analysis, motion tracking and segmentation algorithms are important tools for time-resolved analysis of cell characteristics, events, and tracking. There are many algorithms in everyday use. Nevertheless, most of them is not properly validated as the ground truth (GT), which is a very important tool for the verification of image processing algorithms, is not naturally available. Many algorithms in this field of study are, therefore, validated only manually by an human expert. This is usually difficult, cumbersome and time consuming task, especially when single 3D image or even 3D image sequence is considered.

In this paper, we have proposed a technique that generates time-lapse sequences of fully 3D synthetic image datasets. It includes generating shape, structure, and also motion of selected biological objects. The corresponding GT data is generated as well. The technique is focused on the generation of synthetic objects at various scales. Such datasets can be then processed by selected segmentation or motion tracking algorithms. The results can be compared with the GT and the quality of the applied algorithm can be measured.

Keywords: simulation, optical flow, 3D image sequences, fluorescence optical microscopy.

1 Introduction

The present biomedical research increasingly relies on automated processing and analysis of large amount of numerical or image data, which are nowadays commonly produced by the vast majority of acquisition devices. These devices typically degrade the raw data to some extent. In optical microscopy, for example, the data are blurred by the optical system and, subsequently, affected by various types of noise during the use of digital camera. Two fundamental tasks in this area are image segmentation and motion tracking. The former is typical for the manipulation with static images while the latter manages time-lapse sequences. The task of segmentation is to split the image into several disjoint regions, often reduced to identifying foreground and background ones. The task of motion tracking is focused on tracking of some of these regions. This allows for the description of events and changes in the characteristics of studied objects over a

A. Campilho and M. Kamel (Eds.): ICIAR 2012, Part II, LNCS 7325, pp. 473–482, 2012.
© Springer-Verlag Berlin Heidelberg 2012

period of time. In both cases, the acquired raw image data are processed and we obtain some results. The question is whether these results are correct or not. If the ground truth (GT) image data were available, we could compare the outputs of the examined algorithm with the given GT and, consequently, we could validate the quality of the algorithm. In optical microscopy, the issue is that cells and their components cannot be simply observed with the naked eye, simply without any acquisition device, just like it is in the macroscopic world. Therefore, the original unaffected image, which is essentially the GT, is impossible to obtain. Clearly, one may ask a human expert to annotate her existing images in order to turn them into a GT dataset. But this is very tedious and unreliable, especially in the 3D case. Another particularly popular solution is to make use of simulator, which is a framework for generating pseudo-real GT datasets.

As presented in [27] each simulator can be clearly split into three principal phases: (I) digital phantom object generation, (II) simulation of signal transmission, and (III) simulation of signal detection and image formation. In the first phase (I) the model that fits the observed data is chosen. The model can be either static [11,9,24,26] or dynamic in time [5,8,32,20,23]. It is noteworthy, that these models do not exactly model the simulated reality. That is why one more likely meets the term *phantoms* instead of *models*. The second phase (II) covers the period during which a signal is transmitted through the environment. One of the most typical environment characteristics is the impulse response of the system, often called the point spread function (PSF), which causes blur of the transmitted image data. It can be either a real (empirically measured) PSF [27] or simply Gaussian kernel [9,16,14,24]. Some authors even presume, that the PSF is spatially variant [11]. The last phase (III) corresponds to the detection of the signal with the device sensors and its conversion to the digital representation.

At this point we should emphasize the fact that shortening the time-lapse sequence into just one frame reduces the whole task into the generation of one static synthetic image. Therefore, we can understand the generation of *static* synthetic image data as a subtask of the generation of *time-lapse* sequences.

In the rest of this section we will make a brief survey of the most common simulators in both aspects – static as well as dynamic. In addition, we will group them according to the scale of generated objects.

1.1 State of the Art

From Macromolecules to Microspheres. Regarding the simplest point-like objects such as FISH spots, Grigoryan et al. [9] proposed a simulation toolbox for generating large sets of spots. Each spot was represented by a sphere randomly placed in 3D space. Two individual spheres were allowed to overlap, but only under specific conditions. Manders et al. [16] also addressed the issue of virtual spot generation. They verified a novel region-growing segmentation algorithm over a large set of Gaussian-like 3D objects arranged in a grid. Later Svoboda et al. [26] focused on the generation of microspheres. We would like to point out that not only spherical-like objects (spots, microspheres) can be

simulated at this scale-space. Gene structures were modelled in [3] using the wormlike chain model [10].

In the field of particle-image velocimetry a tool generating standard images was introduced by Okamoto et al. [19] and used, for example, for the validation of algorithms tracking the movement of specific positions of DNA molecules [17].

From Single Nucleus to Cell Populations. Concerning cell-like objects, the vast majority of algorithms responsible for the generation of phantoms uses the simple geometric shapes, such as circles and ellipses in 2D and spheres and ellipsoids in 3D space. To check the quality of the new cell nuclei segmentation algorithm, Lockett et al. [13] generated a set of artificial spatial objects in the shape of curved spheres, ellipsoids, discs, bananas, satellite discs, and dumbbells. In [11] and [15] more complex simulators, that could produce large cell populations, have been designed. However, these toolboxes were designed for 2D images only. Svoboda et al. [26] extended this model to manipulate fully 3D phantom of cell nuclei, but with a limited number of generated objects. The progress was reached in [27] which enabled the generation of large sets of spots and cell populations. Later this approach was extended by incorporating the creation of complex phantoms of human colon tissues [25].

Graner et al. [8] focused on time-lapse generation of large cell populations. They adopted the statistical large-Q Potts model to simulate the reorganization of uniformly distributed cell-like objects to guarantee the natural shape and distribution of the cells. The individual cells were, however, characterized by the shape only, their internal structure was omitted. The generation of synthetic time-lapse sequences was further developed by Dufour et al. [5]. In their work, they focused on both the validation of cell segmentation as well as cell tracking algorithms. They generated phantoms of several touching 3D cells in order to validate the ability of the segmentation algorithms to distinguish between individual cells. The phantoms were then overlaid with blurred additive gaussian noise to mimic intracellular structures and their images further processed to simulate passing through optical and acquisition systems. To test the motion tracking, they positioned the phantoms on trajectories they had generated in advance. It is, however, not clear how they guaranteed the continuity of the internal cell structures in the neighbouring frames. Similar concept was adopted by Gerencser et al. [7] who simulated movement of mitochondria to learn and improve performance of their optical flow method, which they used for study of mitochondrial motility in real images afterwards. They generated 2D image sequences in which mitochondria affected by photon shot noise and signal-to-noise ratio adjustments were moving with a constant speed. Respective parameters were varied between sequences. They modelled mitochondria either as spheres or as elongated cylinders capped with half spheres on both ends.

Unlike the majority of authors who tried to describe the cell shape and structure analytically Zhao et al. [34] designed an algorithm for generating the whole 2D cell, including the nucleus, proteins, and cell membrane, using machine learning from real data. The machine learning approach was also adopted in work by Xiong et al. [33].

Organs. Macroscopic objects like the kidneys, heart, brain, muscles, or blood vessels are examples of objects that are relatively easy to model as their shape and behavior are well understood. The problem is to choose the model that fits observed data to the greatest extent possible. Generation of the static models has already been studied extensively when creating the reference phantom image for the brain [29,21,2]. When handling these types of image data, no movement is expected. Completely different object types represent the heart or blood vessels, where activity is studied and kinetic models [6,22,20,1,28,18] are needed.

1.2 Contribution of This Paper

In this paper, we present a novel technique that offers the generation of static images as well as time-lapse image sequences. Both are fully 3D fluorescence microscopy image data ranging from images of microspheres up to images of tissues accompanied always with GT information. The GT consists of segmentation mask for every image in the sequence and optical flow field for every consecutive pair. Such datasets of static images are, for example, advantageous for performance and comparison studies of segmentation methods. The sequences, on the other hand, are suitable for evaluations of tracking methods. The following section explains the methodology. Then, the application of the proposed technique is presented.

2 Method

2.1 Generation of Static Images

As it has been already mentioned in the first section, each simulator can be split into three consecutive stages: (I) phantom generation, (II) signal transmission, and (III) signal detection and image formation. The first stage can be generally characterized as a collection of particular image processing algorithms that together give rise to an image of a particular phantom. The process is randomized to allow for variability, that is, to allow for obtaining different images of the same simulated object. Clearly, the selection of the algorithms is strongly dependent on the phantom and, for this reason, thorough description of this stage is beyond the scope of this paper. We rather encourage the reader to the more appropriate resources [11,27,25].

The second and the third stages simulate the signal transmitting system and the signal detector, which is in our case an optical fluorescence microscope with a CCD camera. Similarly to Malm et al. [15], the main task of the second stage is to compute convolution with the PSF, which is well-known to be the most dominant source of aberration. This function describes an image of a single point signal as it is transmitted through the microscope. We use an empirically measured one [27]. Besides, we incorporate uneven illumination.

In the last stage we simulate the image formation in the CCD camera, which is typically mounted on modern optical fluorescence microscopes. In particular, we generate the readout noise, the dark charge noise and the photon shot noise.

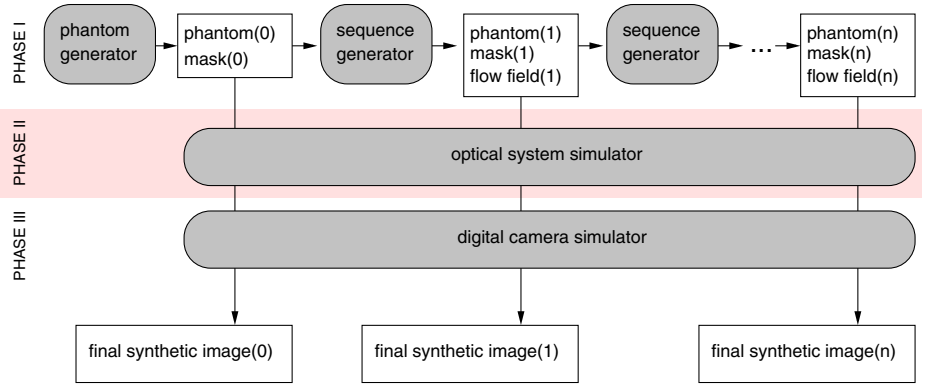

Fig. 1. Scheme of the proposed simulation toolbox. It consists of three subsequent phases depicted vertically. In the first phase, the digital phantom and mask is created. The static phantom, denoted with index (0), may be set in motion to obtain a time-lapse sequence, eventually. The second phase imitates the optical system while the last phase simulates the virtual scanning device (here CCD camera). Only the phantom images are subjected to these two phases. The output of this scheme is either single synthetic image with its mask or time-lapse sequence of synthetic images with their masks and flow fields.

2.2 Generation of Image Sequences

In order to generate time-lapse sequence two engines are employed: phantom generator and sequence generator. The phantom generator (see Section 2.1) is executed only once to create the initial phantom with its binary mask. Afterwards, the phantom is iteratively transformed with sequence generator. Each execution of sequence generator produces the transformed phantom and corresponding binary mask. Moreover, a flow field describing the transformation process is obtained as well. Finally, each phantom in the time-lapse sequence is individually processed in the stages II and III in order to complete the final time-lapse sequence of synthetic image datasets. Refer to Fig. 1 for overview of the proposed technique.

The transformation in sequence generator is achieved by warping the given phantom image according to an artificially generated flow field [12] that mimics the observed movements. Namely, we utilize the backward (image) transformation [12] and piece-wise smooth flow fields [30,4]. Basically, a flow field assigns 3D "shift" vector to every pixel of the image according to which the pixel is "moved" into the next generated image.

The smoothness is important to avoid artifacts during the warping [31]. Also such flow fields may be concatenated [30] so that we may actually obtain any image in the sequence directly from the single phantom image created at the beginning of the simulation. As a result, time-lapse continuity of shape and structure in the generated images is preserved (see Fig. 2). Moreover, the phantom

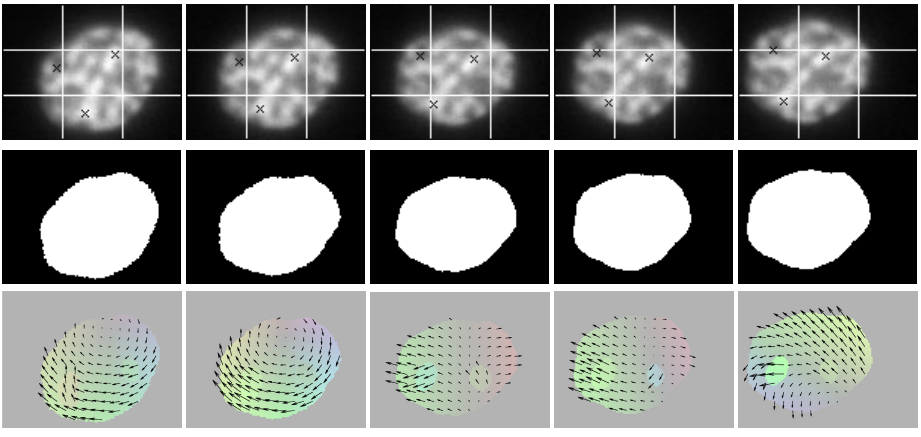

(a) t=1 (b) t=6 (c) t=13 (d) t=22 (e) t=31

Fig. 2. Sample images with GT from an artificially generated time-lapse observation of a nucleus of HL60 cell. In top row, only the middle xy-slice of the 3D image is shown. The whole sequence consisted of 30 images from which only 5, in which capabilities of the proposed technique are clearly exhibited, are shown. We additionally overlaid images with the white grid, which is stationary, and with the crosses, which are following movement of the nucleus, to facilitate observation of the present movements. The associated GT masks and GT flow fields are shown in the middle and bottom rows, respectively. The vectors are enhanced for clarity. Colour-encoded flow fields are shown underneath the vectors. Note that the nucleus included two nucleoli that move independently. Their movements are best observed with the patches present in the GT flow fields, which also outline their positions.

image is warped exactly once, which reduces the amount of warping artifacts to the least possible extent. Note that the 3D shift vectors may be real allowing for warping at sub-pixel accuracy. In fact, we use this concept in two independent layers, that is, two phantom images and two smooth flow fields, that are put to move individually and that ar merged together in the end to produce resulting image of the sequence (see Fig. 2). A significantly different movement of, for example, some intracellular compartment compared to the movement of the rest of the cell can be simulated in this way.

We simulate full 3D rotation and translation with the generated flow fields in our implementation of the method. We also incorporate linear stretching of a rectangular 3D volume by defining flow vector at every of the 8 vertices of the volume. The rest of the flow field is linearly interpolated from these vectors. Such flow field is capable of producing effects such as magnification, shrinking, shearing, etc. In fact, we combine these to simulate real movement. Targeting at evaluation of tracking methods, this concept accommodate both the registration-based and optical flow-based tracking methods. The generated GT can be used not only to verify the result of tracking, that is, the tracks of given objects, but also to verify intermediate results of the methods. For instance, we may encode image transformation (translation, affine, etc.) into the flow field and verify

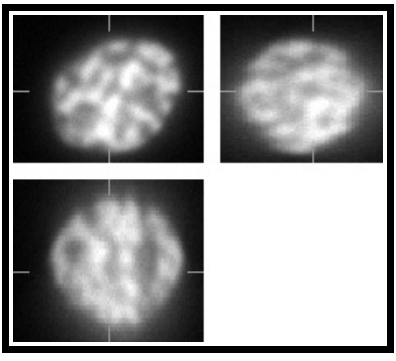

Fig. 3. Initial static synthetically generated image with one HL-60 nucleus inside. This 3D figure consists of three individual images: the top-left image contains a selected xy-slice, the top-right image corresponds to a selected yz-slice, and the bottom one depicts a selected xz-slice. Three mutually orthogonal slice planes are shown with ticks.

whether the registration method in question recovered correct parameters of the transformation. Results of optical flow computing methods can be compared directly.

Last but not least, we remind that the whole process works in 3D image space. This is, however, an improvement over the traditional methods [31], to the best of our knowledge, for producing optical flow datasets with GT as these are based on different assumptions; for example, specular reflectance of observed objects or perspective projection of 3D world to 2D imaging plane [31].

3 Application

We have implemented the proposed technique. For the purpose of the presentation of the results, we have selected to generate time-lapse observation of a nucleus of HL60 cell line. However, the technique is not limited to this cell line only. Adaptation of the technique to different object type and size is only a matter of changing its parameters, in contrast to changing its design. Sample cross-section of a generated 3D image showing nucleus of a HL60 cell is depicted in Fig. 3. This image was set in motion. For the illustration of the generated sequence refer to Fig. 2. A video made from the sequence of generated images can be downloaded from our Information System[1]. The plausibility of generated nucleus was examined in our previous work [27]. We have also previously demonstrated [30,31] that the generating image sequences based on warping of still the same image according to piece-wise smooth flow fields does not introduce unexpected artifacts, additional noise or other unwanted distortion to the image content. In other words, we have managed to generate long image sequences of constant visual quality. In this particular test, the parameters of the movements

[1] `http://is.muni.cz/www/4203/HL60demo.avi`

were set based on our observation and experience. They were varying in time to mimic, sort of, shivering of the nucleus. In addition, we simulated dominant translational and rotational movement of it.

4 Conclusion

We presented a novel simulation technique. It is capable of generating static images as well as time-lapse image sequences of fully 3D fluorescence microscopy image data accompanied with ground truth. Here, the ground truth is represented by binary image masks and flow fields to aid the evaluation of segmentation and tracking methods, respectively. The flow fields were used to repetitively transform the initial image in order to obtain the final image sequence. The important property of the proposed technique is that it preserves time-lapse continuity of shape and structure in the generated images and reduces the amount of image distortion to the least possible extent. Currently, our implementation can simulate the time-lapse images showing motion of objects of various sizes, for example, individual GFP probes, HL60 cell line nuclei, granulocytes or cell clusters.

Acknowledgment. This research was supported by the Grant Agency of the Czech Republic (Grant No. P302/12/G157).

References

1. Arts, T., Hunter, W.C., Douglas, A., Muijtjens, A.M., Reneman, R.S.: Description of the deformation of the left ventricle by a kinematic model. Journal of Biomechanics 25(10), 1119–1127 (1992)
2. Aubert-Broche, B., Griffin, M., Pike, G.B., Evans, A.C., Collins, D.L.: Twenty new digital brain phantoms for creation of validation image data bases. IEEE Trans. Med. Imaging 25(11), 1410–1416 (2006)
3. Baddeley, D., Weiland, Y., Batram, C., Birk, U., Cremer, C.: Model based precision structural measurements on barely resolved objects. Journal of Microscopy 237(1), 70–78 (2010)
4. Black, M.J., Anandan, P.: The robust estimation of multiple motions: parametric and piecewise-smooth flow fields. Comput. Vis. Image Underst. 63(1), 75–104 (1996)
5. Dufour, A., Shinin, V., Tajbakhsh, S., Guillen-Aghion, N., Olivo-Marin, J.C., Zimmer, C.: Segmenting and tracking fluorescent cells in dynamic 3-D microscopy with coupled active surfaces. IEEE Transactions on Image Processing 14(9), 1396–1410 (2005)
6. Flores-Tapia, D., Thomas, G., Sabouni, A., Noghanian, S., Pistorius, S.: Breast tumor microwave simulator based on a radar signal model. In: International Symposium on Signal Processing and Information Technology, pp. 17–22 (2006)
7. Gerencser, A.A., Nicholls, D.G.: Measurement of instantaneous velocity vectors of organelle transport: Mitochondrial transport and bioenergetics in hippocampal neurons. Biophysical Journal 95, 3070–3099 (2008)
8. Graner, F., Glazier, J.A.: Simulation of biological cell sorting using a two-dimensional extended Potts model. Phys. Rev. Lett. 69(13), 2013–2016 (1992)

9. Grigoryan, A.M., Hostetter, G., Kallioniemi, O., Dougherty, E.R.: Simulation toolbox for 3D-FISH spot-counting algorithms. Real-Time Imaging 8(3), 203–212 (2002)
10. Kratky, O., Porod, G.: Röntgenuntersuchung Gelöster Fadenmoleküle. Recueil des Travaux Chimiques des Pays-Bas-J. of the Royal Netherlands Chemical Society 68(12), 1106–1122 (1949)
11. Lehmussola, A., Ruusuvuori, P., Selinummi, J., Huttunen, H., Yli-Harja, O.: Computational framework for simulating fluorescence microscope images with cell populations. IEEE Trans. Med. Imaging 26(7), 1010–1016 (2007)
12. Lin, T., Barron, J.L.: Image reconstruction error for optical flow. In: Vision Interface, pp. 73–80 (1994)
13. Lockett, S.J., Sudar, D., Thompson, C.T., Pinkel, D., Gray, J.W.: Efficient, interactive, and three-dimensional segmentation of cell nuclei in thick tissue sections. Cytometry 31, 275–286 (1998)
14. Ma, Y., Kamber, M., Evans, A.C.: 3D simulation of PET brain images using segmented MRI data and positron tomograph characteristics. In: Computerized Medical Imaging and Graphics, vol. 17, pp. 365–371 (1993)
15. Malm, P., Brun, A., Bengtsson, E.: Papsynth: simulated bright-field images of cervical smears. In: Proceedings of the 2010 IEEE International Conference on Biomedical Imaging: From Nano to Macro, ISBI 2010, pp. 117–120. IEEE Press (2010)
16. Manders, E.M.M., Hoebe, R., Strackee, J., Vossepoel, A.M., Aten, J.A.: Largest contour segmentation: A tool for the localization of spots in confocal images. Cytometry 23, 15–21 (1996)
17. Matov, A., Edvall, M.M., Yang, G., Danuser, G.: Optimal-flow minimum-cost correspondence assignment in particle flow tracking. Computer Vision and Image Understanding 115(4), 531–540 (2011)
18. Moore, J., Drangova, M., Wierzbicki, M., Barron, J.L., Peters, T.: A High Resolution Dynamic Heart Model Based on Averaged MRI Data. In: Ellis, R.E., Peters, T.M. (eds.) MICCAI 2003. LNCS, vol. 2878, pp. 549–555. Springer, Heidelberg (2003)
19. Okamoto, K., Nishio, S., Saga, T., Kobayashi, T.: Standard images for particle-image velocimetry. Measurement Science and Technology 11(6), 685 (2000)
20. Rabben, S.I., Haukanes, A.L., Irgens, F.: A kinematic model for simulating physiological left ventricular deformation patterns – a tool for evaluation of myocardial strain imaging. In: IEEE Symposium on Ultrasonics, vol. 1, pp. 134–137 (2003) ISBN: 0-7803-7922-5
21. Rexilius, J., Hahn, H.K., Bourquain, H., Peitgen, H.O.: Ground Truth in MS Lesion Volumetry – A Phantom Study. In: Ellis, R.E., Peters, T.M. (eds.) MICCAI 2003. LNCS, vol. 2879, pp. 546–553. Springer, Heidelberg (2003)
22. Schlaikjer, M., Torp-Pedersen, S., Jensen, J., Stetson, P.: Tissue motion in blood velocity estimation and its simulation. In: Proc. 1998 IEEE Ultrasonics, Symposium, p. 1495 (1998)
23. Schlaikjer, M., Torp-Pedersen, S., Jensen, J.A.: Simulation of RF data with tissue motion for optimizing stationary echo canceling filters. Ultrasonics 41, 415–419 (2003)
24. Solórzano, C.O.d., Rodriguez, E.G., Jones, A., Pinkel, D., Gray, J.W., Sudar, D., Lockett, S.J.: Segmentation of confocal microscope images of cell nuclei in thick tissue sections. Journal of Microscopy 193, 212–226 (1999)

25. Svoboda, D., Homola, O., Stejskal, S.: Generation of 3D Digital Phantoms of Colon Tissue. In: Kamel, M., Campilho, A. (eds.) ICIAR 2011, Part II. LNCS, vol. 6754, pp. 31–39. Springer, Heidelberg (2011)
26. Svoboda, D., Kašík, M., Maška, M., Hubený, J., Stejskal, S., Zimmermann, M.: On Simulating 3D Fluorescent Microscope Images. In: Kropatsch, W.G., Kampel, M., Hanbury, A. (eds.) CAIP 2007. LNCS, vol. 4673, pp. 309–316. Springer, Heidelberg (2007)
27. Svoboda, D., Kozubek, M., Stejskal, S.: Generation of digital phantoms of cell nuclei and simulation of image formation in 3d image cytometry. Cytometry part A 75A(6), 494–509 (2009)
28. Tavakoli, V., Sahba, N., Ahmadian, A., Alirezaie, J.: An evaluation of different optical flow techniques for myocardial motion analysis in B-Mode echocardiography images. In: 4th Kuala Lumpur International Conference on Biomedical Engineering 2008, IFMBE Proceedings, vol. 21, pp. 506–510. Springer, Heidelberg (2008)
29. Tofts, P., Barker, G., Filippi, M., Gawne-Cain, M., Lai, M.: An oblique cylinder contrast-adjusted (OCCA) phantom to measure the accuracy of MRI brain lesion volume estimation schemes in multiple sclerosis. Magnetic Resonance Imaging 15(10), 183–192 (1997)
30. Ulman, V., Hubený, J.: Pseudo-real Image Sequence Generator for Optical Flow Computations. In: Ersbøll, B.K., Pedersen, K.S. (eds.) SCIA 2007. LNCS, vol. 4522, pp. 976–985. Springer, Heidelberg (2007)
31. Ulman, V.: Fast Anisotropic Filtering and Performance Evaluation Tool for Optical Flow in Biomedical Image Analysis. Ph.D. thesis, Masaryk University (2011)
32. Waks, E., Prince, J.L., Douglas, A.S.: Cardiac motion simulator for tagged MRI. In: MMBIA 1996: Proceedings of the 1996 Workshop on Mathematical Methods in Biomedical Image Analysis (MMBIA 1996), p. 182. IEEE Computer Society, Washington, DC (1996)
33. Xiong, W., Wang, Y., Ong, S.H., Lim, J.H., Jiang, L.: Learning cell geometry models for cell image simulation: An unbiased approach. In: ICIP, pp. 1897–1900 (2010)
34. Zhao, T., Murphy, R.F.: Automated learning of generative models for subcellular location: Building blocks for systems biology. Cytometry Part A 71A(12), 978–990 (2007)